Association of the Cystic Fibrosis Transmembrane Regulator with CAL: Structural Features and Molecular Dynamics†

Andrea Piserchio,‡ Abigail Fellows,§ Dean R. Madden,*,§ and Dale F. Mierke*,‡

Department of Molecular Pharmacology, Division of Biology and Medicine, Brown University, Providence, Rhode Island 02912, and Department of Biochemistry, Dartmouth Medical School, Hanover, New Hampshire 03755

Received August 18, 2005; Revised Manuscript Received October 6, 2005

ABSTRACT: The association of the cystic fibrosis transmembrane regulator (CFTR) with two PDZ-containing molecular scaffolds (CAL and EBP50) plays an important role in CFTR trafficking and membrane maintenance. The CFTR−molecular scaffold interaction is mediated by the association of the C-terminus of the transmembrane regulator with the PDZ domains. Here, we characterize the structure and dynamics of the PDZ of CAL and the complex formed with CFTR employing high-resolution NMR. On the basis of NMR relaxation data, the α2 helix as well as the $\beta2-\beta3$ loop of CAL PDZ domain undergoes rapid dynamics. Molecular dynamics simulations suggest a concerted motion between the α2 helix and the $\beta1-\beta2$ and $\beta2-\beta3$ loops, elements which define the binding pocket, suggesting that dynamics may play a role in PDZ−ligand specificity. The C-terminus of CFTR binds to CAL with the final four residues ($-D^{-3}$-T-R-L^{0}) within the canonical PDZ-binding motif, between the β2 strand and the α2 helix. The R^{-1} and D^{-3} side chains make a number of contacts with the PDZ domain; many of these interactions differ from those in the CFTR−EBP50 complex, suggesting sites that can be targeted in the development of PDZ-selective inhibitors that may help modulate CFTR function.

Cystic fibrosis (CF)[1] is a common lethal autosomal recessive genetic disorder, generally correlated with abnormal Cl^- conductance at the plasma membrane of epithelial cells, resulting in the disruption of fluid and ion homeostasis. The disease is caused by mutations occurring in the cystic fibrosis transmembrane conductance regulator (CFTR) gene (*1*−*3*), the most common of which is the deletion of phenylalanine 508 (ΔF508). CFTR is a transmembrane protein located mainly on the apical surface of epithelial cells (*4*, *5*) and functions as a cAMP-regulated, ATP-gated chloride channel (*6*−*8*). Like many other glycoproteins, CFTR assembles in the endoplasmatic reticulum, matures in the Golgi apparatus, and is finally delivered to the plasma membrane (see ref *9* for a review). The protein is internalized from the plasma membrane into endosomes and then, depending on a complex set of regulatory interactions, either recycled back to the cell surface or directed to lysosomes for degradation (*10*−*12*). CFTR can thus be eliminated either by the ER quality control (*13*) or by endosome-mediated internalization mechanisms (*10*). Misfolded or unstable CFTR mutants are rapidly degraded through both pathways, with a consequent lack of channels on the cell surface.

Recently, two distinct molecules, EBP50 (50 kDa ezrin-binding protein, also known as NHERF1, Na^+/H^+ exchange regulatory factor-1) and CAL [CFTR-associated ligand, also known as PIST (PDZ protein interacting specifically with TC10), GOPC (Golgi-associated PDZ and coiled-coil protein), and FIG (fused in glioblastoma)], both PDZ (PSD-95, Discs-large, Zo-1) domain-containing proteins, have been implicated in the regulation of CFTR trafficking. EBP50 is localized at the apical surface; it includes two PDZ motifs, both of which bind CFTR (*14*). Through EBP50, CFTR is tethered to the cytoskeleton actin filaments (*15*) and couples with both the β2 adrenergic receptor and protein kinase A (*16*). CAL, on the other hand, has a single PDZ domain that specifically binds the C-terminus of CFTR (*17*). CAL is mainly localized at the trans-Golgi network (TGN) (*17*) and to smaller extents at the plasma membrane and in lysosomes (*10*), although its localization has recently been shown to depend on interactions with the Rho-GTPase TC10 (*18*).

The steady-state level of mature CFTR depends on CAL in a concentration-dependent manner (*17*). In cells overexpressing CAL, a drop in the level of CFTR expression is observed at the plasma membrane, as well as in the overall cell. Importantly, the concomitant overexpression of EBP50 restores the original CFTR concentration and distribution (*17*). These data are consistent with a model in which EBP50 and CAL compete for binding to the CFTR C-terminus. CAL-mediated reduction of CFTR levels can also be reversed

† This work was supported, in part, by National Institutes of Health Grants GM-54082 (D.F.M.) and P20 RR018787 from the IDeA Program (D.R.M.), by the Cystic Fibrosis Foundation (D.F.M. and D.R.M.), and by Howard Hughes Medical Institute Grant 76200-560801 to Dartmouth Medical School (D.R.M.).

* To whom correspondence should be addressed. D.F.M.: Department of Molecular Pharmacology, Division of Biology and Medicine, Box G-B4, Brown University, Providence, RI 02912; phone, (401) 863-2139; fax, (401) 863-1595; e-mail, dale_mierke@brown.edu. D.R.M.: Department of Biochemistry, Dartmouth Medical School, 7200 Vail Building, Hanover, NH 03755; phone, (603) 650-1164; fax, (603) 650-1128; e-mail, drm0001@dartmouth.edu.

‡ Brown University.

§ Dartmouth Medical School.

[1] Abbreviations: CAL, CFTR-associated ligand; CF, cystic fibrosis; CFTR, cystic fibrosis transmembrane conductance regulator; DTT, dithiothreitol; EBP50, 50 kDa ezrin-binding protein; PDZ, PSD-95, Discs-large, Zo-1; TGN, trans-Golgi network.

10.1021/bi0516475 CCC: $30.25
Published on Web 11/12/2005

by simultaneous overexpression of a constitutively active form of TC10, which leads to a redistribution of CAL from the TGN toward the plasma membrane (*18*). Considering these findings, the PDZ domain of CAL may be a key target for regulating CFTR trafficking. A molecule able to selectively bind the CAL PDZ domain without altering EBP50−CFTR association would represent an attractive tool for dissecting the complex mechanisms of CFTR trafficking, and for testing the hypothesis that CAL inhibition could enhance CFTR delivery at the plasma membrane, initially suggested by Cheng and co-workers (*10*, *17*).

While the structure of the complex formed by the C-terminus of CFTR with EBP50 has already been described (*19*), that formed with CAL is still unknown. Here, we characterize by solution NMR spectroscopy and computational methods the structure and dynamics of the CAL PDZ domain and its interaction with the C-terminus of CFTR. The analysis reveals several differences between the EBP50 and CAL binding interactions, which may serve as targets for the design of specific inhibitors.

MATERIALS AND METHODS

Sample Preparation. The peptide (Glu^{-7}-Glu^{-6}-Val^{-5}-Gln^{-4}-Asp^{-3}-Thr^{-2}-Arg^{-1}-Leu^{0}) containing the C-terminus of CFTR was purchased from the Tufts University (Boston, MA) core facility. The CAL (AF450008) PDZ domain was expressed as a decahistidine fusion protein. Isotopically labeled proteins were expressed in M9 minimal medium containing 1× BME vitamins (Sigma), 4 mg/L thiamine (VWR), and either 1% (w/v) glucose (Fisher) or 0.4% (w/v) [^{13}C]glucose (Spectra Stable Isotopes). $^{15}NH_4Cl$ was used to prepare M9 salts for ^{15}N labeling. Following metal-affinity and size-exclusion chromatography, protein was concentrated to approximately 1.5 mM in a volume of 300 μL. The resulting samples were dialyzed against a 50 mM phosphate buffer [40 mM NaCl and 10 mM dithiothreitol (DTT) (pH 5.5)] and transferred to Shigemi NMR tubes. A high DTT concentration was required to prevent protein precipitation. The NMR samples containing the ligand were prepared by adding solid peptide to the concentrated protein solution to yield peptide:protein molar ratios of up to 8:1.

NMR Spectroscopy. All NMR experiments were performed at 25 °C on a Bruker Avance 600 MHz spectrometer equipped with a triple-resonance probe and a triple-axis gradient unit. TSP was used as direct proton reference and as an indirect ^{13}C and ^{15}N reference. Backbone assignment was achieved through standard two-dimensional (2D) ^{1}H−^{15}N HSQC, three-dimensional (3D) CBCA(CO)NH, 3D HNCO, 3D HN(CO)CA, 3D HBHA(CO)NH, and 3D HNCA experiments, while 3D HC(C)H-TOCSY and 3D HC(C)H-COSY experiments were employed for the aliphatic side chain assignment. Aromatic frequencies were identified using 2D ^{1}H−^{1}H NOESY and 3D ^{1}H−^{1}H NOESY−^{13}C HSQC experiments. Distance restraints for the CAL PDZ domain were obtained from 2D ^{1}H−^{1}H NOESY, 3D ^{1}H−^{1}H NOESY−^{13}C HSQC, and 3D ^{1}H−^{1}H NOESY−^{15}N HSQC experiments with mixing times ranging between 80 and 100 ms. ^{15}N HSQC spectra were collected every 5 °C between 10 and 35 °C to determine [^{1}H]amide temperature coefficients. Intermolecular NOEs between the protein and the ligand were obtained using 2D ^{13}C double-half-filtered NOESY experiments, with mixing times between 80 and 130 ms. The ^{1}H peptide chemical shift assignment was obtained through 2D ^{15}N-filtered TOCSY and NOESY experiments.

Relaxation measurements were performed using inversion recovery (R_1), CPMG (R_2), and steady-state ^{1}H−^{15}N NOE experiments. A 4 s recycling delay and a 9.4 × 40 Hz/point resolution (prior to zero filling) were employed for all the relaxation experiments. For R_1 measurements, eight inversion recovery experiments with delays ranging between 11.1 and 710.4 ms were employed; 11 delays between 16.3 and 179.3 ms were used to calculate R_2. Fitting of the data was done using a Levenberg−Marquardt routine and the following simple exponential:

$$I(t) = A\mathrm{e}^{-R_{1,2}t} \tag{1}$$

The reduced spectral density functions were calculated using the equations

$$\begin{bmatrix} J(0) \\ J(\omega_N) \\ J_{avg}(\omega_H) \end{bmatrix} = \begin{bmatrix} \frac{3}{4E} & \frac{3}{2E} & \frac{-9}{10E} \\ \frac{1}{E} & 0 & \frac{-7}{5E} \\ 0 & 0 & \frac{1}{5A} \end{bmatrix} \times \begin{bmatrix} R_1 \\ R_2 \\ R_{NOE} \end{bmatrix} \tag{2}$$

$$R_{NOE} = (\mathrm{NOE} - 1)R_1(\gamma_N/\gamma_H) \quad \mathrm{NOE} = \frac{I_{SAT}}{I_{eq}} \tag{3}$$

$$A = (\mu_0/4\pi)^2(\gamma_H\gamma_N\hbar^2/4r_{NH}^6) \quad B = (\Delta^2\omega_N^2) \qquad E = 3A + B \tag{4}$$

where μ_0 is the vacuum permeability and Δ is the chemical shift anisotropy (−160 ppm). All the NMR spectra were processed with NMRPipe (*20*) and analyzed with Sparky (*21*).

Structure Calculations. Dihedral angle restraints were obtained using TALOS (*22*). Backbone hydrogen bonds were deduced by inspection of the temperature coefficients and implemented as ambiguous distance restraints. Similarly, side chain chemical shift perturbations were included in the calculations as intermolecular distance restraints by assuming a distance of 3.0 Å between the perturbed protein moiety and an unspecified portion of the ligand. The NOE intensities were converted into distances using an r^{-6} dependency assuming an error of 40% to accommodate all possible uncertainties. Ambiguous NOEs or unassigned peaks were introduced into an ARIA (*23*) protocol, including a final refinement step with explicit solvent (*24*) run with CNS (*25*). The resulting structures were analyzed using ProcheckNMR and ProFit (*26*).

Molecular Dynamics. The GROMACS (*27*) package was employed to run all the MD calculations and analyze the trajectories. The simulations were 3 ns long, and the OPLS force field was used (*28*). The protein starting conformation was randomly chosen among the low-energy NMR structures. The protein was soaked with SPC water molecules (*29*) in an octahedral box having a 5.5 nm periodic image distance. A time step of 1 fs was used for velocity integration. The neighboring list was updated every 10 steps using a grid search; twin range cutoffs of 1.4 and 1.2 nm were used for Coulomb-like and van der Waals interactions, respectively.

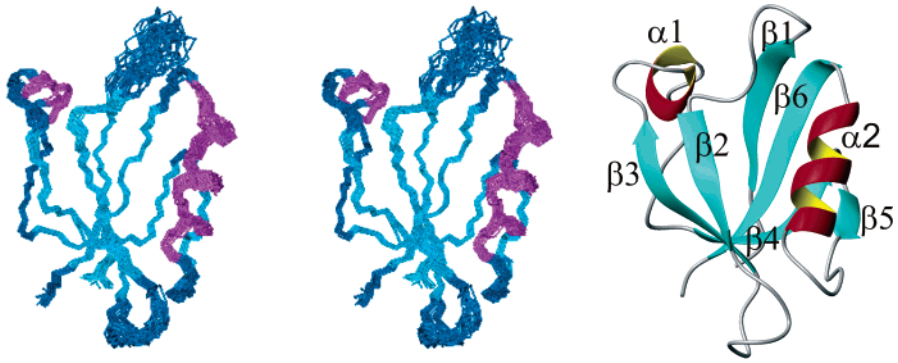

FIGURE 1: Structure of the PDZ domain of CAL. At the left is a stereoview using the backbone (Cα, C, and N) atoms. The α-helices are colored magenta and the β-strands aqua. At the right is a secondary structure representation.

To reproduce the charge shielding encountered in the high-salt concentration buffers, sodium and chlorine ions were added to neutralize each charged side chain. Temperature and pressure coupling were imposed to 300 K and 1 bar using time constants of 20 fs and 1 ps, respectively, through a Berendsen thermostat (*30*). Experimental NOEs were applied as time-averaged restraints using a 100 fs time constant and a 1000 kJ mol^{-1} nm^{-2} force constant. For principal component analysis, the Cα atom coordinates along the trajectory were fit to an average structure, and the covariance matrix was then calculated:

$$C_{ij} = \langle (x_i - \langle x_i \rangle)(x_j - \langle x_i \rangle) \rangle$$

The matrix was diagonalized, providing the principal modes (eigenvectors) and their corresponding eigenvalues. The principal components are the projection of the data on the eigenvectors:

$$\mathbf{p} = \mathbf{R}^T(\mathbf{x} - \langle \mathbf{x} \rangle)$$

where **R** is the matrix of eigenvectors.

RESULTS

Determination of the NMR Assignment and Structure of the CAL PDZ Domain. At the millimolar concentrations employed for the NMR experiments, the CAL PDZ domain is partially aggregated, as indicated by the relatively long apparent correlation time (trimmed average of 10.5 ns calculated from the R_2/R_1 ratios) and size exclusion chromatography elution time (data not shown). Even at lower protein concentrations (~50 μM), aggregation (line broadening) was still evident, although to a lesser extent. Importantly, the spectra do not indicate any structural differences, or differences in ligand binding, as the concentration is increased. Nevertheless, despite the consequent low quality of the NMR spectra, the majority of the backbone and side chain resonances of the PDZ domain (residues 278−362) have been assigned. Exceptions are the amides of residues located in the β1−β2 loop (H^{288} and E^{289}), at the beginning of the β2 strand (L^{291}, G^{292}, and I^{293}), and in the β2−β3 loop (E^{300}), which could not be detected in any ^{15}N HSQC-like experiment. Approximately 13.5 distance restraints per residue were obtained from NOESY experiments, and 102 dihedral restraints were derived from the chemical shifts. For 31 backbone amide protons, hydrogen bonding interactions were identified from temperature coefficients (*31*). From these data, 15 structures fulfilling the experimental restraints were generated (Figure 1). On the basis of the statistical analysis of the backbone dihedral angles and hydrogen bonds (*26*, *32*), the ensemble of NMR structures has a resolution of 2.2 Å.

The overall three-dimensional fold does not diverge significantly from the canonical PDZ arrangement, characterized by two α-helices and six antiparallel β-strands organized into a β-sandwich-like scaffold (Figure 1). These secondary structure elements are well-defined (rmsd of 0.50 Å fitting backbone heavy atoms against an average structure), although the C-terminal end of the α2 helix appears to be less ordered (rmsd of 0.8 Å). The resolution drops significantly in the loops; the backbone dihedral angles found in the disallowed (1.9% of the total) and generously allowed regions (2.7%) of the Ramachandran plot originate in these portions of the molecule. Although the loops are less well-resolved, they do contain well-defined local structural elements, including β-turns, specifically in the β3−α1 loop (P^{312}-G^{313}), α1−β4 loop (V^{324}-G^{325}), and β4−β5 loop (N^{332}-G^{333}). Additionally, in more than half of the ensemble of structures, β-turns are observed in the β1−β2 (D^{287}-H^{288}) and β2−β3 (K^{299}-E^{300} and H^{301}-G^{302}) loops.

NMR Relaxation Studies of the CAL PDZ Domain. Relaxation rates have been measured for 61 residues, as illustrated in Figure 2. As mentioned above, both longitudinal and axial relaxation constants are abnormally high for a protein in the 12 kDa range. Interestingly, the R_1 values are sequence-dependent (commonly observed for R_2 and NOE). The particularly high R_2 value observed for T^{296} immediately suggests the presence of chemical exchange. Fitting the data with the model-free approach (*33*−*36*) produced order parameters close to 1 with generally poor "goodness of fit" for all models tested. This formalism has a number of advantages; however, it cannot be applied if the molecule exhibits aggregation (*37*), as is the case here.

Reduced spectral density mapping was then employed for a more qualitative analysis of the data (*38*−*45*). The $J(0)$ function is characterized by quite uniformly high values, with the exception of that of T^{296}. Chemical exchange is certainly associated with T^{296} and is most likely affecting those residues in the β1−β2 loop and β2 strand whose amides can be observed in the bound conformation, but not in the free protein. Lower-than-average $J(0)$ values are observed for the large α1−β4 and α2−β6 loops. As anticipated, the patterns for $J(\omega_N)$ and $J(\omega_H)$ are the opposite of those observed for $J(0)$ (*46*). This is particularly evident in the case of the $J(\omega_N)$ function, where values are generally lower

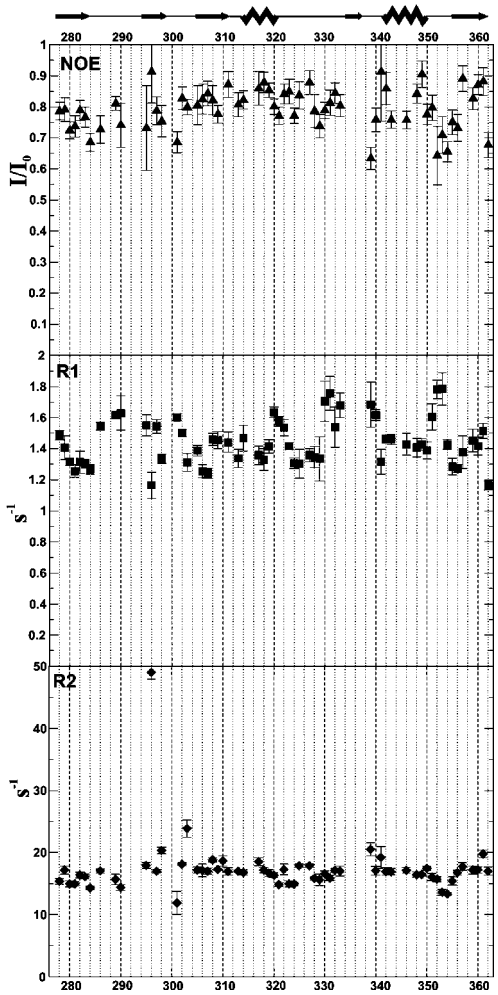

FIGURE 2: NMR relaxation data (NOE, R_1, and R_2) measured for the PDZ domain of CAL correlated with the secondary structure elements.

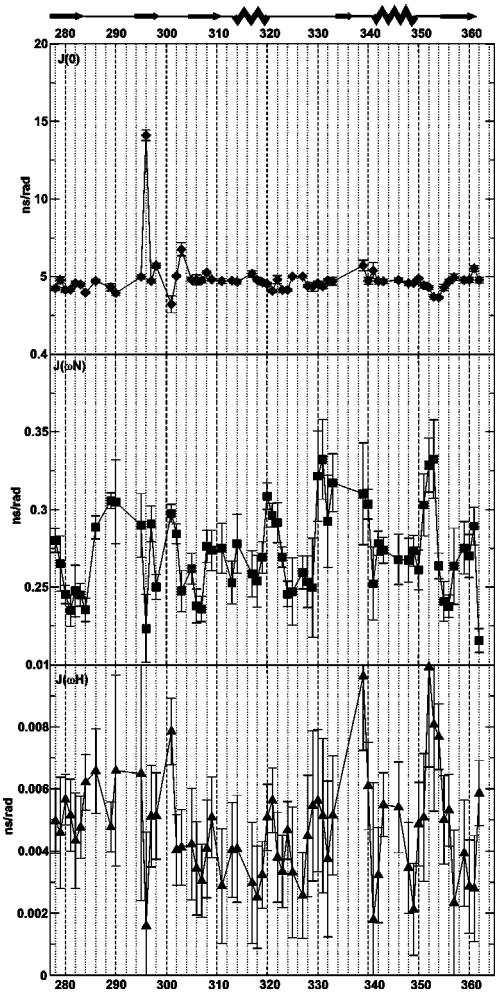

FIGURE 3: Reduced spectral density functions [$J(0)$, $J(\omega_N)$, and $J_{avg}(\omega_H)$], measured for the PDZ domain of CAL.

in the core of the regular secondary structure motifs and increase as one enters the loops. A careful analysis of the $J_{avg}(\omega_H)$ function is more difficult, as in many cases the uncertainty is on the same order of magnitude as the calculated spectral density values; however, in general, a pattern similar to that for $J(\omega_N)$ is observed.

Molecular Dynamic Simulations of the CAL PDZ Domain. The PDZ domain does not undergo any major structural changes during the 3 ns simulation, illustrated by an rmsd for the Cα atoms of 1.1 Å. The secondary structural motifs are well-conserved for the entire simulation, although the N- and C-terminal residues of the α-helices undergo transitions between the α-helix and β-turn-like conformations. In the $\beta2-\beta3$ loop, residues $K^{299}-V^{293}$ oscillate among turn, 3_{10}, and coil conformations, consistent with the variability observed within the ensemble of structures obtained from the NMR refinement.

The MD simulations complement the experimental sampling of molecular motions and dynamics. The main limit of this approach is the accuracy of the force field and, more importantly, the length of the simulations (*47*). Therefore, in the analysis of the 3 ns trajectory carried out here using principal component analysis (*48*−*51*), we focus on the higher-amplitude fluctuations of the protein and limit our analysis to a qualitative description of the motions. As described by Hess (*52*), the diagonalization of the covariance matrix (in our case restricted to the Cα atoms) generates a new reference system where the covariance is zero for each couple of coordinates. The eigenvalue represents the displacement (variance) along the direction defined by the corresponding eigenvector. In this way, the biologically relevant motions typically characterized by wider amplitudes and therefore higher eigenvalues can be isolated from the lower-amplitude fluctuations. The projections of the trajectory on the eigenvectors are called principal modes, while the structural changes related to an eigenvector can be inspected by filtering the trajectory along that direction.

Approximately 60% of the total fluctuations are included within the first five eigenvalues (Figure 4). The first principal component is associated with conformational changes of several loops (mainly $\beta1-\beta2$, $\beta2-\beta3$, and $\beta5-\alpha2$) and a rearrangement of both helices with respect to the protein core (Figure 5). As is often the case, the cosine content for this transition is high (0.8), suggesting a random diffusion behavior (*52*, *53*). The time evolution of the principal components is illustrated in Figure 6. The remaining principal components display a number of amplitude motions in the nanosecond to picosecond time scale. For example, a twist of the α2 helical axis with respect to the $\beta2$ strand can be observed in the trajectory filtered in the direction of the second principal component (Figure 7). Similarly, the translation of α2 with respect to the protein core is highlighted by the third eigenvector. Frequent rearrangements

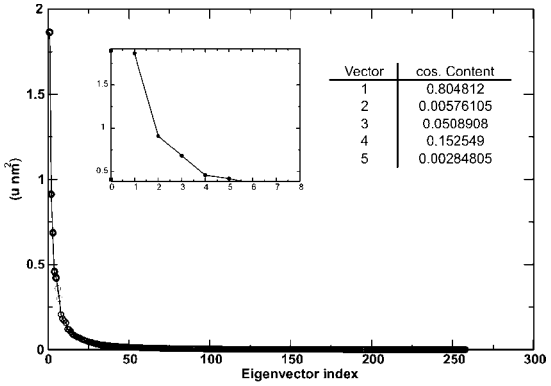

FIGURE 4: Eigenvalues calculated from the diagonalization of the covariance matrix. The five largest eigenvalues representative of the wider molecular motions and their cosine content are highlighted.

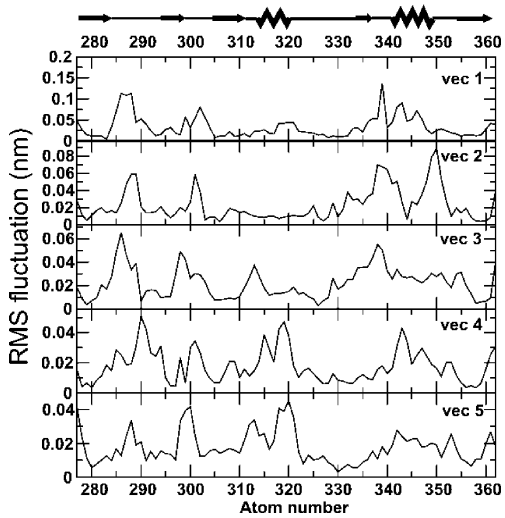

FIGURE 5: Maximum rmsd values as a function of the protein sequence of the principal components with the five largest eigenvalues. The larger rmsd values indicate larger fluctuations for that particular molecular motion.

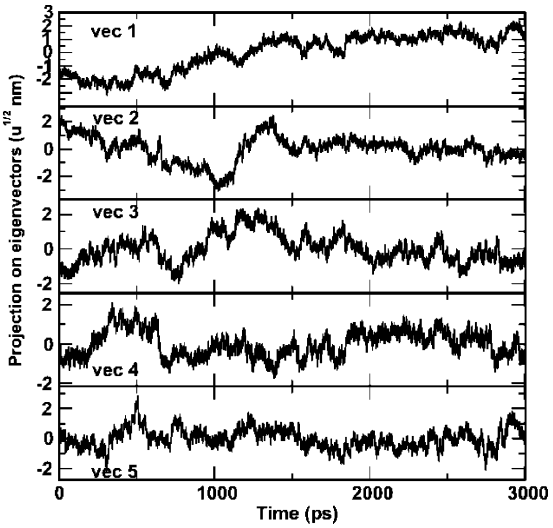

FIGURE 6: Time evolution for the principal components characterized by the five largest eigenvalues. The first principal component shows a cosine-like shape, while a number of conformational transitions can be found for the other principle components.

or distortions of the helical loops are also observed for the other two principal components; however, the amplitudes

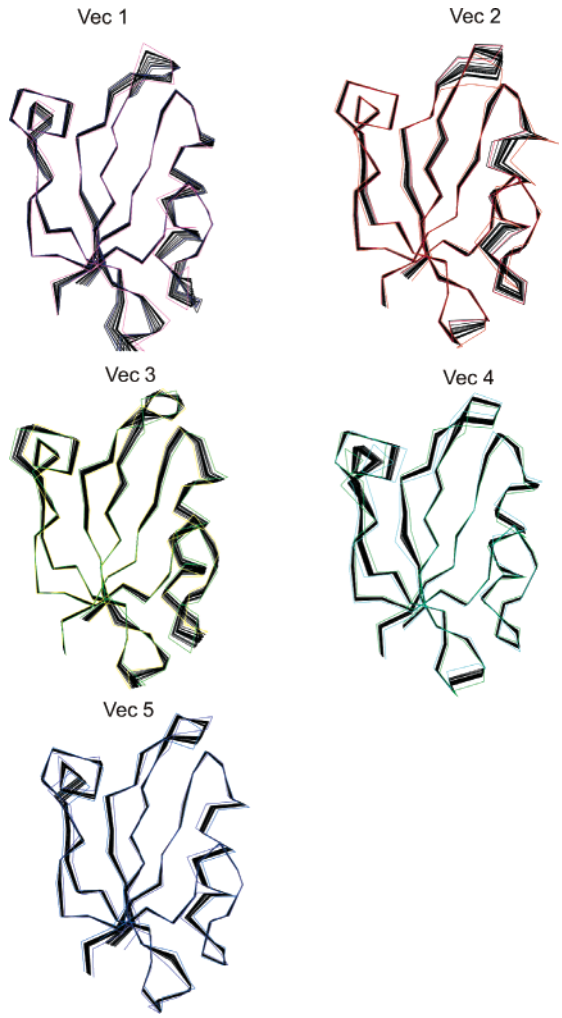

FIGURE 7: Projections of the MD trajectory on the eigenvector with the five largest eigenvalues. Twenty structures (Cα atoms only) are sampled, and the wider fluctuations are color-coded.

of the motions are significantly decreased, and are more homogeneously distributed along the entire backbone.

Structure of the CAL PDZ Domain−CFTR Complex. The constant for binding of the CAL PDZ domain and the CFTR C-terminus could not be determined with high accuracy because of CAL oligomerization. The NMR spectra are consistent with a system in the slow-to-fast exchange regime, with one set of complete resonances for both the free and bound forms, with accentuated broadening of the ligand peaks. The interaction with the peptide perturbs the NMR frequencies of the PDZ domain. The most evident is the appearance of all of the amide resonances that could not be detected for the PDZ domain alone (located in strand $\beta 2$ and in the $\beta 1-\beta 2$ and $\beta 2-\beta 3$ loops). In general, most of the $^{1}H-^{15}N$ peaks are altered by the binding, with the largest changes localized on the $\beta 2$ and $\beta 3$ strands, on the $\alpha 1$ and $\alpha 2$ helices, and in the $\beta 1-\beta 2$ and $\beta 2-\beta 3$ loops. The side chain resonances are likewise altered, with pronounced perturbations for residues in $\beta 2$ and $\alpha 2$, and isolated residues in the $\beta 2-\beta 3$ loop (H^{291}), $\beta 3$ strand (E^{309} and H^{311}), and even the $\beta 5-\alpha 2$ loop (T^{339}).

A large number of CFTR−CAL intermolecular NOEs (*49*) have been unambiguously identified (only a single NOE was observed between the CFTR peptide and the PDZ backbone, Arg^{-1} Hα−S^{294} Hα). Most of the intermolecular interactions

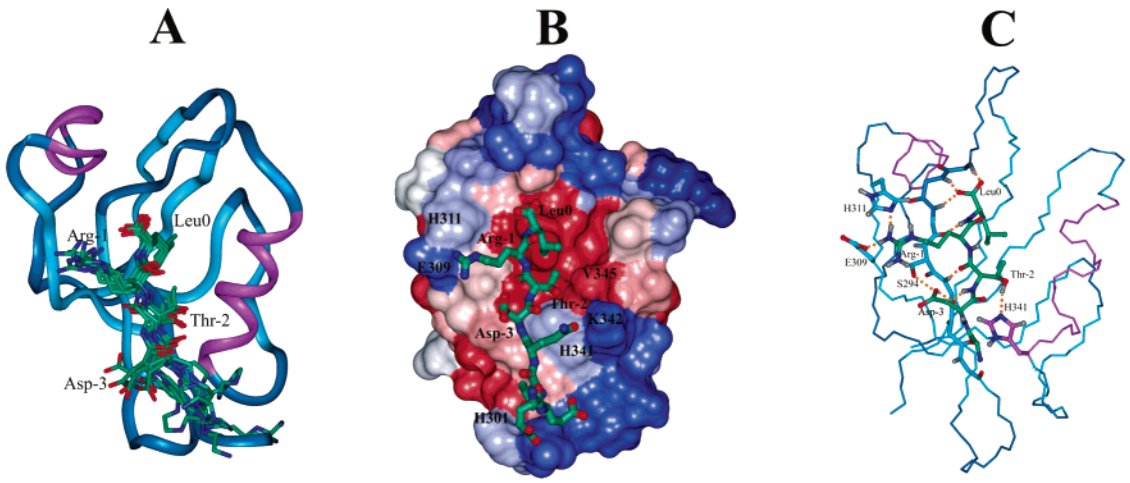

FIGURE 8: (A) Different possible orientations of the CFTR peptide in the CAL binding pocket derived exclusively from NMR restraints. The ligand is depicted in ball-and-stick format. (B) Interactions between CAL and the CFTR peptide as obtained from the MD simulations after equilibration and application of the NMR-derived restraints. The surface of the PDZ domain is depicted as a solid surface, with hydrophobic residues colored red and hydrophilic residues blue. The large hydrophobic binding pocket hosting both the Leu^0 and Thr^{-2} methyl groups can be easily identified. Residues relevant to the CAL−CFTR interactions are denoted. (C) Hydrogen bonds between CAL and CFTR obtained from NMR chemical shift perturbations and MD calculations.

involve the side chains of Leu^0, Thr^{-2}, and Asp^{-3}; no NOEs were observed for Arg^{-1} or the N-terminal residues beyond Asp^{-3}. These data, together with chemical shift perturbations, were introduced into the calculation protocol previously described, and the results are shown in Figure 8. The C-terminus of the peptide is inserted with an extended conformation between β2 and α2. The orientations of the Leu^0 and Thr^{-2} side chains, both directed toward α2, are well-defined. Despite the lack of NOEs, the ambiguous restraints are sufficient to locate the Arg^{-1} side chain between E^{309} and H^{311} on β3, while the Asp^{-3} carboxylic group is relatively poorly defined. The lack of NOE restraints does not allow for structural characterization of the peptide beyond position −5. However, the N-terminus of the peptide would be in position to interact with K^{342} (α2 helix), T^{339} (β5−α2 loop), and H^{301} (β2−β3 loop), all of which exhibit chemical shift perturbation upon addition of the peptide.

MD Simulations of the CAL PDZ Domain−CFTR Complex. Molecular dynamics simulations were carried out to further refine the CAL−CFTR association. During the initial portion of the simulation, the backbone of the CFTR peptide is relatively more flexible than the protein, until approximately 1.5 ns in which the peptide, from Leu^0 to Gln^{-4}, converges toward a β-sheet conformation and forms stable hydrogen bonds with β2 (Figure 8). During the simulation, the side chains of Leu^0 and Thr^{-2} are stable within their respective binding pockets, while Arg^{-1} and Asp^{-3} are more flexible. Residue Arg^{-1} interacts with E^{309} and H^{311} of β3 (Figure 8). The interaction of the side chain carboxylic group of Asp^{-3} is less well defined with hydrogen bonds to S^{292} (β2 strand) and internally to Arg^{-1} observed, in addition to interactions with H^{301} (β2−β3 loop) and K^{342} (α2).

DISCUSSION

PDZ domains are ubiquitous molecular modules acting as scaffolds, mediating protein−protein interactions in several biological events. The PDZ fold is extremely well conserved in nature, and indeed, the CAL three-dimensional structure derived here does not diverge from it significantly. In particular, the CAL and EBP50 PDZ domains are very similar, with an rmsd of 1.1 Å for the secondary structural elements (heavy atoms of the helices and strands). The binding affinity for PDZ domains is weak (typically dissociation constants in the micromolar range are measured), when compared for instance with that of canonical hormone−receptor interactions. Such weak binding can be associated with the role of PDZ domains, which must bind their target proteins only for the time necessary to induce a subsequent protein−protein interaction or increase the level of cellular compartment localization. Unfortunately, such affinities make the structural characterization of PDZ domain−ligand complexes challenging, as the complexes are difficult to crystallize and intermolecular NOEs observed via NMR are limited. In this NMR investigation, these difficulties were overcome by using a combination of experimental data (direct protein−peptide NOE contacts and indirect contacts via chemical shift perturbations) and extensive computational methods (MD simulations).

Furthermore, it is increasingly appreciated that dynamic changes in the ligand-binding pocket can play an important role in regulating potential interactions. For example, the orientation of the α2 helix is believed to be particularly important in determining the ligand specificity of PDZ domains, and a correlation between the geometry of the second helix and the PDZ selectivity at the −2 position has been reported (*54*). Recently, Vuister and co-workers showed how in two variants of the second PDZ domain of PTP-BL the dynamic properties of the β2−β3 loop regulate the binding affinity by reorienting the α2 helix (*55*, *56*). Indeed, backbone amide perturbation in the β2−β3 loop is often observed in NMR studies of PDZ domains (*18*, *57*). Thus, in addition to overcoming weak affinity, a biophysical understanding of the binding of CFTR to the CAL PDZ domain requires parallel consideration of binding site dynamics.

Here, the internal mobility of the CAL PDZ domain was characterized by NMR relaxation data and the reduced spectral densities as introduced by Wagner and co-workers (*38*−*41*). In short, $J(0)$ probes motions on the nanosecond to millisecond time scale, while both $J(\omega_N)$ and $J_{avg}(\omega_H)$ are

sensitive to fast picosecond fluctuations (*46*). On the basis of this analysis, the $\beta2-\beta3$ loop is undergoing efficient averaging on both the picosecond (H^{291}) and microsecond to millisecond (V^{293}) time scales. Furthermore, on average, the entire α2 helix shows more motions on the picosecond time scale [larger $J(\omega_N)$ and $J(\omega_H)$] than the other secondary structure elements.

These experimental observations are complemented by the results from the MD simulation and principal component analysis. The modes associated with the higher eigenvalues are constantly characterized by relatively wide fluctuations in the $\beta2-\beta3$ loop. They are localized in the correspondence of the labile turns previously described and are coupled with more subtle changes in the α2 helix involving helical axis translation and reorientation, as well as distortions of the individual helical turns. These motions appear to be in the nanosecond range, with the exception of the first principal component, which is certainly not equilibrated [high cosine content (*52*, *53*)] and for which the simulation length represents just a lower limit. The long time scales are consistent with the complexity of the molecular motions, involving rearrangement of the tertiary structure together with the distortion of secondary structure elements.

Overall, all of our data are consistent with the PDZ binding pocket being quite dynamic, with the relative orientation of the two most important binding determinants ($\beta2$ strand and α2 helix) connected by the dynamics of the $\beta2-\beta3$ loop. A certain degree of flexibility is not unusual in binding regions and is often required for ligand recognition.

The structural features of the CAL−CFTR complex were determined employing the NOE and amide chemical shift perturbation data and refined with MD simulations, providing an unequivocal description of the peptide orientation (up to residue −4) in the PDZ binding pocket. It is common that only the C-terminal residues within the binding cleft are structurally resolved, by either X-ray or NMR analysis. In accord with this observation, deletion of the residues up to residue −4 of CFTR abolishes the association with CAL (*18*). The results closely resemble those for the familiar PDZ domain−ligand interaction: the peptide main chain is adjoined to the $\beta2$ strand and thus forms an extension of the antiparallel β-sheet, while the peptide carboxyl terminus hydrogen bonds to the amides of the $\beta1-\beta2$ loop (Figure 8). The Leu^0 side chain is tightly packed in the characteristic hydrophobic cavity situated between the end of the α2 helix and the $\beta1-\beta2$ loop. In the CAL PDZ domain, this surface is relatively wide (approximately 200 $Å^2$) and better suited for large hydrophobic side chains (Ile and Leu in comparison to Val). Similarly, the methyl group of Thr^{-2} is tightly packed against the V^{319} moiety located in the core of α2. A similar contact has been identified in other PDZ domains (*58*) and appears as a general determinant in stabilizing the Thr amino acid at the −2 position. Belonging to the class I family, the CAL PDZ domain presents a His residue at the beginning of the α2 helix (H^{301}) whose side chain projects into the binding region. In our study, the imidazole group is clearly affected by the peptide binding, and H-bond formation with the Thr^{-2} hydroxyl group is suggested by the MD simulations. On the opposite side of the binding groove, the side chains of residues Arg^{-1} and Asp^{-3} are oriented toward the β-sheet surface and consequently more solvent exposed, resulting in a small number of distance restraints.

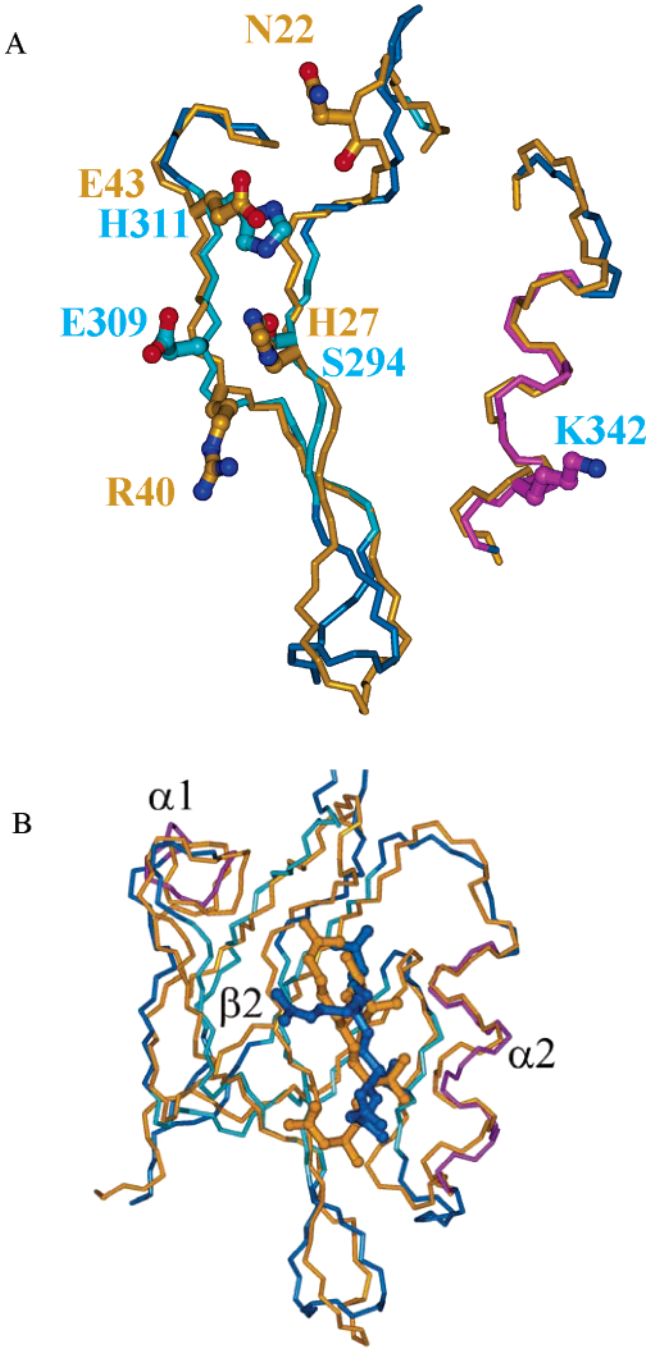

FIGURE 9: Arg^{-1} and Asp^{-3} binding pockets. Comparison between NHERF1 and CAL PDZ domains. CAL is color-coded (magenta for helices and aqua for strands), and NHERF is colored gold. The side chains directly involved in the CFTR interactions are shown in ball-and-stick format.

In short, our data indicate that Leu^0 and Thr^{-2} are indeed responsible for most of the affinity, which is reflected in the dominant role of these positions in the type I PDZ binding motif. Nevertheless, the side chains of Arg^{-1} and Asp^{-3} also recognize specific binding pockets. The $\beta2-\beta3$ loop plays a role in the process as well, most likely through the H^{301} imidazole, but the mechanism is unclear due to the lack of NOE restraints for the N-terminal region of the ligand.

A detailed comparison of the binding interaction of the CFTR C-terminus with the PDZ domains of CAL and EBP50 (Figure 9) can provide insight into differences that might permit the targeted design of selective inhibitors (*59*−*61*). In both cases, the side chains of the four terminal residues

bind to the PDZ domain (*19*, *62*), with Leu^0 accommodated in a broad hydrophobic pocket and Arg^{-1} stabilized by intra- and intermolecular salt bridges and hydrogen bonds. The lack of crystallographic evidence for binding of Gln^{-4} to EBP50 PDZ1 is consistent with our NMR data for the CAL PDZ domain, which also fail to reveal specific interactions upstream of Asp^{-3}. There are also a number of significant differences. In the CAL PDZ domain, the binding pocket for Arg^{-1} is located at the end of the β3 strand, while in EBP50, the side chain is reoriented toward the β3−α1 loop (Figure 9B). Furthermore, Asp^{-3} engages in different interactions in the two PDZ domains. In EBP50, it makes contacts with a His and an Arg residues on β2 and β3, respectively. In CAL, Asp^{-3} interacts with S^{294} and, although less clearly, with K^{342}, which are not conserved in EBP50. An unambiguous NOE was also identified between the T^{296} methyl group and Asp^{-3} methylene protons, and a specific interaction between the hydroxyl of T^{296} and the carboxylate of Asp^{-3} was observed during the MD simulations. In CAL, mutation of these side chains, together with K^{340}, has been shown to dramatically reduce the affinity of the PDZ domain without disrupting its overall structure (M. Wolde et al., manuscript in preparation). Notably, the side chains of these residues project toward the solvent in the absence of CFTR, suggesting that the drop in the affinity of the mutants originates from the removal of direct contact with the C-terminal peptide.

In conclusion, this work elucidates aspects of the structure and dynamics of the CAL PDZ domain both in the absence of ligand and while associated with the C-terminus of CFTR. Taken together, our results suggest that efforts to develop molecules that can discriminate between the PDZ domains of CAL and EBP50 should focus on improving the interaction with the β-strands, which "tune" the affinity for the natural ligands, while not disrupting the internal hydrophobic pocket of the PDZ domain responsible for most of the binding affinity. We postulate that insight from such investigations, combined with similar efforts targeting EBP50, will lead to novel strategies for regulating CFTR expression at the cell surface.

ACKNOWLEDGMENT

We acknowledge the assistance of Jessica Plati and Maria Pellegrini in the course of these studies and the helpful comments of John Marshall (Brown University). We also gratefully acknowledge the collaborative support of Dr. Bruce Stanton (Dartmouth Medical School) and Dr. William Guggino (The Johns Hopkins University School of Medicine, Baltimore, MD) in initiating this project.

REFERENCES

1. Riordan, J. R., Rommens, J. M., Kerem, B., Alon, N., Rozmahel, R., Grzelczak, Z., Zielenski, J., Lok, S., Plavsic, N., Chou, J. L., et al. (1989) Identification of the cystic fibrosis gene: Cloning and characterization of complementary DNA, *Science 245*, 1066−73.
2. Rommens, J. M., Iannuzzi, M. C., Kerem, B., Drumm, M. L., Melmer, G., Dean, M., Rozmahel, R., Cole, J. L., Kennedy, D., Hidaka, N., et al. (1989) Identification of the cystic fibrosis gene: Chromosome walking and jumping, *Science 245*, 1059−65.
3. Kerem, B., Rommens, J. M., Buchanan, J. A., Markiewicz, D., Cox, T. K., Chakravarti, A., Buchwald, M., and Tsui, L. C. (1989) Identification of the cystic fibrosis gene: Genetic analysis, *Science 245*, 1073−80.
4. Ames, G. F., Mimura, C. S., and Shyamala, V. (1990) Bacterial periplasmic permeases belong to a family of transport proteins operating from *Escherichia coli* to human: Traffic ATPases, *FEMS Microbiol. Rev. 6*, 429−46.
5. Hyde, S. C., Emsley, P., Hartshorn, M. J., Mimmack, M. M., Gileadi, U., Pearce, S. R., Gallagher, M. P., Gill, D. R., Hubbard, R. E., and Higgins, C. F. (1990) Structural model of ATP-binding proteins associated with cystic fibrosis, multidrug resistance and bacterial transport, *Nature 346*, 362−5.
6. Anderson, M. P., Rich, D. P., Gregory, R. J., Smith, A. E., and Welsh, M. J. (1991) Generation of cAMP-activated chloride currents by expression of CFTR, *Science 251*, 679−82.
7. Anderson, M. P., Gregory, R. J., Thompson, S., Souza, D. W., Paul, S., Mulligan, R. C., Smith, A. E., and Welsh, M. J. (1991) Demonstration that CFTR is a chloride channel by alteration of its anion selectivity, *Science 253*, 202−5.
8. Bear, C. E., Duguay, F., Naismith, A. L., Kartner, N., Hanrahan, J. W., and Riordan, J. R. (1991) Cl^- channel activity in *Xenopus* oocytes expressing the cystic fibrosis gene, *J. Biol. Chem. 266*, 19142−5.
9. Kopito, R. R. (1999) Biosynthesis and degradation of CFTR, *Physiol. Rev. 79*, S167−73.
10. Cheng, J., Wang, H., and Guggino, W. B. (2004) Modulation of mature cystic fibrosis transmembrane regulator protein by the PDZ domain protein CAL, *J. Biol. Chem. 279*, 1892−8.
11. Gentzsch, M., Chang, X. B., Cui, L., Wu, Y., Ozols, V. V., Choudhury, A., Pagano, R. E., and Riordan, J. R. (2004) Endocytic trafficking routes of wild type and ΔF508 cystic fibrosis transmembrane conductance regulator, *Mol. Biol. Cell 15*, 2684−96.
12. Bradbury, N. A., Clark, J. A., Watkins, S. C., Widnell, C. C., Smith, H. S. T., and Bridges, R. J. (1999) Characterization of the internalization pathways for the cystic fibrosis transmembrane conductance regulator, *Am. J. Physiol. 276*, L659−68.
13. Ward, C. L., Omura, S., and Kopito, R. R. (1995) Degradation of CFTR by the ubiquitin-proteasome pathway, *Cell 83*, 121−7.
14. Raghuram, V., Mak, D. D., and Foskett, J. K. (2001) Regulation of cystic fibrosis transmembrane conductance regulator single-channel gating by bivalent PDZ-domain-mediated interaction, *Proc. Natl. Acad. Sci. U.S.A. 98*, 1300−5.
15. Short, D. B., Trotter, K. W., Reczek, D., Kreda, S. M., Bretscher, A., Boucher, R. C., Stutts, M. J., and Milgram, S. L. (1998) An apical PDZ protein anchors the cystic fibrosis transmembrane conductance regulator to the cytoskeleton, *J. Biol. Chem. 273*, 19797−801.
16. Naren, A. P., Cobb, B., Li, C., Roy, K., Nelson, D., Heda, G. D., Liao, J., Kirk, K. L., Sorscher, E. J., Hanrahan, J., and Clancy, J. P. (2003) A macromolecular complex of β2 adrenergic receptor, CFTR, and ezrin/radixin/moesin-binding phosphoprotein 50 is regulated by PKA, *Proc. Natl. Acad. Sci. U.S.A. 100*, 342−6.
17. Cheng, J., Moyer, B. D., Milewski, M., Loffing, J., Ikeda, M., Mickle, J. E., Cutting, G. R., Li, M., Stanton, B. A., and Guggino, W. B. (2002) A Golgi-associated PDZ domain protein modulates cystic fibrosis transmembrane regulator plasma membrane expression, *J. Biol. Chem. 277*, 3520−9.
18. Cheng, J., Wang, H., and Guggino, W. B. (2005) Regulation of cystic fibrosis transmembrane regulator trafficking and protein expression by a Rho family small GTPase TC10, *J. Biol. Chem. 280*, 3731−9.
19. Ladias, J. A. (2003) Structural insights into the CFTR-NHERF interaction, *J. Membr. Biol. 192*, 79−88.
20. Delaglio, F., Grzesiek, S., Vuister, G. W., Zhu, G., Pfeifer, J., and Bax, A. (1995) NMRPipe: A multidimensional spectral processing system based on UNIX pipes, *J. Biomol. NMR 6*, 277−93.
21. Goddard, T. D., and Kneller, D. G. (2001) Sparky 3.0, University of California, San Francisco.
22. Cornilescu, G., Delaglio, F., and Bax, A. (1999) Protein backbone angle restraints from searching a database for chemical shift and sequence homology, *J. Biomol. NMR 13*, 289−302.
23. Nilges, M., Macias, M. J., O'Donoghue, S. I., and Oschkinat, H. (1997) Automated NOESY interpretation with ambiguous distance restraints: The refined NMR solution structure of the pleckstrin homology domain from β-spectrin, *J. Mol. Biol. 269*, 408−22.
24. Linge, J. P., Williams, M. A., Spronk, C. A., Bonvin, A. M., and Nilges, M. (2003) Refinement of protein structures in explicit solvent, *Proteins 50*, 496−506.

25. Brunger, A. T., Adams, P. D., Clore, G. M., DeLano, W. L., Gros, P., Grosse-Kunstleve, R. W., Jiang, J. S., Kuszewski, J., Nilges, M., Pannu, N. S., Read, R. J., Rice, L. M., Simonson, T., and Warren, G. L. (1998) Crystallography & NMR system: A new software suite for macromolecular structure determination, *Acta Crystallogr. D54*, 905−21.
26. Laskowski, R. A., Rullmannn, J. A., MacArthur, M. W., Kaptein, R., and Thornton, J. M. (1996) AQUA and PROCHECK-NMR: Programs for checking the quality of protein structures solved by NMR, *J. Biomol. NMR 8*, 477−86.
27. Lindahl, E., Hess, B., and van der Spoel, D. (2001) GROMACS 3.0: A package for molecular simulation and trajectory analysis, *J. Mol. Model. 7*, 306−17.
28. Jorgensen, W. L., Maxwell, D. S., and Tirado-Rives, J. (1996) Development and Testing of the OPLS All-Atom Force Field on Conformational Energetics and Properties of Organic Liquids, *J. Am. Chem. Soc. 118*, 11225−36.
29. Berendsen, H. J. C., Postma, J. P. M., van Gunsteren, W. F., and Hermans, J. (1981) in *Intermolecular forces*, pp 331−42, D. Reidel Publishing Co., Dordrecht, The Netherlands.
30. Berendsen, H. J. C., Postma, J. P. M., DiNola, A., and Haak, J. R. (1984) Molecular dynamics with coupling to an external bath, *J. Chem. Phys. 81*, 3684−90.
31. Cordier, F., and Grzesiek, S. (2002) Temperature-dependence of protein hydrogen bond properties as studied by high-resolution NMR, *J. Mol. Biol. 317*, 739−52.
32. Morris, A. L., MacArthur, M. W., Hutchinson, E. G., and Thornton, J. M. (1992) Stereochemical quality of protein structure coordinates, *Proteins 12*, 345−64.
33. Lipari, G., and Szabo, A. (1982) Model-free approach to the interpretation of nuclear magnetic resonance relaxation in macromolecules. 1. Theory and range of validity, *J. Am. Chem. Soc. 104*, 4546−59.
34. Lipari, G., and Szabo, A. (1982) Model-free approach to the interpretation of nuclear magnetic resonance relaxation in macromolecules. 2. Analysis of experimental results, *J. Am. Chem. Soc. 104*, 4559−70.
35. Clore, G. M., Szabo, A., Bax, A., Kay, L. E., Driscoll, P. C., and Gronenborn, A. M. (1990) Deviations from the simple two-parameter model-free approach to the interpretation of nitrogen-15 nuclear magnetic relaxation of proteins, *J. Am. Chem. Soc. 112*, 4989−91.
36. Clore, G. M., Driscoll, P. C., Wingfield, P. T., and Gronenborn, A. M. (1990) Analysis of the backbone dynamics of interleukin-1b using two-dimensional inverse detected heteronuclear nitrogen-15-proton NMR spectroscopy, *Biochemistry 29*, 7387−401.
37. Schurr, J. M., Babcock, H. P., and Fujimoto, B. S. (1994) A test of the model-free formulas. Effects of anisotropic rotational diffusion and dimerization, *J. Magn. Reson., Ser. B 105*, 211−24.
38. Peng, J. W., and Wagner, G. (1995) Frequency spectrum of NH bonds in eglin c from spectral density mapping at multiple fields, *Biochemistry 34*, 16733−52.
39. Lefevre, J. F., Dayie, K. T., Peng, J. W., and Wagner, G. (1996) Internal mobility in the partially folded DNA binding and dimerization domains of GAL4: NMR analysis of the N−H spectral density functions, *Biochemistry 35*, 2674−86.
40. Ishima, R., and Nagayama, K. (1995) Protein backbone dynamics revealed by quasi spectral density function analysis of amide N-15 nuclei, *Biochemistry 34*, 3162−71.
41. Farrow, N. A., Zhang, O., Szabo, A., Torchia, D. A., and Kay, L. E. (1995) Spectral density function mapping using ^{15}N relaxation data exclusively, *J. Biomol. NMR 6*, 153−62.
42. Peng, J. W., and Wagner, G. (1994) Investigation of protein motions via relaxation measurements, *Methods Enzymol. 239*, 563−96.
43. Peng, J. W., and Wagner, G. (1994) Protein mobility from multiple ^{15}N relaxation parameters, *Understanding Chem. React. 8*, 373−454.
44. Peng, J. W., and Wagner, G. (1992) Mapping of spectral density functions using heteronuclear NMR relaxation measurements, *J. Magn. Reson. 98*, 308−32.
45. Peng, J. W., and Wagner, G. (1992) Mapping of the spectral densities of nitrogen−hydrogen bond motions in eglin c using heteronuclear relaxation experiments, *Biochemistry 31*, 8571−86.
46. Dayie, K. T., Wagner, G., and Lefevre, J.-F. (1996) Theory and practice of nuclear spin relaxation in proteins, *Annu. Rev. Phys. Chem. 47*, 243−82.
47. Case, D. A. (2002) Molecular dynamics and NMR spin relaxation in proteins, *Acc. Chem. Res. 35*, 325−31.
48. Levy, R. M., Srinivasan, A. R., Olson, W. K., and McCammon, J. A. (1984) Quasi-harmonic method for studying very low-frequency modes in proteins, *Biopolymers 23*, 1099−112.
49. Garcia, A. E. (1992) Large-amplitude nonlinear motions in proteins, *Phys. Rev. Lett. 68*, 2696−9.
50. Garcia, A. E., and Harman, J. G. (1996) Simulations of CRP: $(cAMP)_2$ in noncrystalline environments show a subunit transition from the open to the closed conformation, *Protein Sci. 5*, 62−71.
51. Amadei, A., Linssen, A. B. M., and Berendsen, H. J. C. (1993) Essential dynamics of proteins, *Proteins: Struct., Funct., Genet. 17*, 412−25.
52. Hess, B. (2000) Similarities between principal components of protein dynamics and random diffusion, *Phys. Rev. E: Stat. Phys., Plasmas, Fluids, Relat. Interdiscip. Top. 62*, 8438−48.
53. Hess, B. (2002) Convergence of sampling in protein simulations, *Phys. Rev. E: Stat., Nonlinear, Soft Matter Phys. 65*, 031910/1−10.
54. Reina, J., Lacroix, E., Hobson, S. D., Fernandez-Ballester, G., Rybin, V., Schwab, M. S., Serrano, L., and Gonzalez, C. (2002) Computer-aided design of a PDZ domain to recognize new target sequences, *Nat. Struct. Biol. 9*, 621−7.
55. Walma, T., Aelen, J., Nabuurs, S. B., Oostendorp, M., van den Berk, L., Hendriks, W., and Vuister, G. W. (2004) A closed binding pocket and global destabilization modify the binding properties of an alternatively spliced form of the second PDZ domain of PTP-BL, *Structure 12*, 11−20.
56. Walma, T., Spronk, C. A., Tessari, M., Aelen, J., Schepens, J., Hendriks, W., and Vuister, G. W. (2002) Structure, dynamics and binding characteristics of the second PDZ domain of PTP-BL, *J. Mol. Biol. 316*, 1101−10.
57. Piserchio, A., Pellegrini, M., Mehta, S., Blackman, S. M., Garcia, E. P., Marshall, J., and Mierke, D. F. (2002) The PDZ1 domain of SAP90. Characterization of structure and binding, *J. Biol. Chem. 277*, 6967−73.
58. Piserchio, A., Salinas, G. D., Li, T., Marshall, J., Spaller, M. R., and Mierke, D. F. (2004) Targeting specific PDZ domains of PSD-95: Structural basis for enhanced affinity and enzymatic stability of a cyclic peptide, *Chem. Biol. 11*, 469−73.
59. Karthikeyan, S., Leung, T., and Ladias, J. A. (2002) Structural determinants of the Na^+/H^+ exchanger regulatory factor interaction with the β2 adrenergic and platelet-derived growth factor receptors, *J. Biol. Chem. 277*, 18973−8.
60. Karthikeyan, S., Leung, T., Birrane, G., Webster, G., and Ladias, J. A. (2001) Crystal structure of the PDZ1 domain of human Na^+/H^+ exchanger regulatory factor provides insights into the mechanism of carboxyl-terminal leucine recognition by class I PDZ domains, *J. Mol. Biol. 308*, 963−73.
61. Webster, G., Leung, T., Karthikeyan, S., Birrane, G., and Ladias, J. A. (2001) Crystallographic characterization of the PDZ1 domain of the human Na^+/H^+ exchanger regulatory factor, *Acta Crystallogr. D57*, 714−6.
62. Karthikeyan, S., Leung, T., and Ladias, J. A. (2001) Structural basis of the Na^+/H^+ exchanger regulatory factor PDZ1 interaction with the carboxyl-terminal region of the cystic fibrosis transmembrane conductance regulator, *J. Biol. Chem. 276*, 19683−6.

BI0516475